

**Synaptic mechanism of differential projections from the
insular and medial prefrontal cortices to the nucleus
accumbens core revealed by optogenetics**

Kensuke Hirose

Nihon University Graduate School of Dentistry

Major in Pediatric Dentistry

(Directors: Profs. Tetsuo Shirakawa and Masayuki Kobayashi,
and Assist. Prof. Yuka Nakaya)

Index

Abstract	-----	2
Introduction	-----	3
Materials and Methods	-----	4
Results	-----	7
Discussion	-----	13
Acknowledgments	-----	16
References	-----	17
Figures	-----	20

This thesis is based on the following article and the additional results in terms of the effects of neostigmine and muscarinic antagonist on light-evoked EPSCs (Fig. 7).

Kensuke Hirose, Yuka Nakaya, Kohei Kitano, Yasuhiko Saito, Ryosuke Kaneko, Yuchio Yanagawa, Kiyofumi Yamamoto, Tetsuo Shirakawa, Masayuki Kobayashi (2021) Differential regulation of medium spiny and cholinergic neurons in the nucleus accumbens core by the insular and medial prefrontal cortices in the rat. *Pfugers Archiv*, 473, 1911-1924.

Abstract

The nucleus accumbens (NAc) receives cortical projections principally from the insular cortex (IC) and medial prefrontal cortex (mPFC). Among NAc neurons, cholinergic interneurons (ChNs) regulate the activities of medium spiny neurons (MSNs), which make up ~95% of NAc neurons, by modulating their firing and synaptic properties. However, little is known about the synaptic mechanisms, including their cell-type-dependent corticoaccumbal projection properties and cholinergic effects on the NAc core. Here, I performed whole-cell patch-clamp recordings from NAc, MSNs, and ChNs in acute brain slice preparations obtained from rats that received an AAV5-hSyn-ChR2(H134R)-mCherry injection into the IC or mPFC. Light stimulation of IC or mPFC axons induced comparable phase-locked excitatory postsynaptic currents (EPSCs) in MSNs. On the other hand, ChNs showed consistent EPSCs evoked by light stimulation of mPFC axons, whereas light stimulation of IC axons evoked much smaller EPSCs, which often showed failure in ChNs. Light-evoked EPSCs were abolished by tetrodotoxin, which were recovered by 4-aminopyridine, suggesting that corticoaccumbal projections monosynaptically induce EPSCs in MSNs and ChNs. Carbachol effectively suppressed the amplitude of EPSCs in MSNs and ChNs evoked by light stimulation of IC or mPFC axons and in ChNs evoked by stimulating mPFC axons. Neostigmine mimicked this cholinergic suppression of EPSCs. The carbachol-induced suppression was recovered by atropine or pirenzepine, while preapplication of M₂ allosteric modulators gallamine, M₃ receptor antagonist J104129, M₄ receptor antagonist PD102807, or M₂/M₄ receptor antagonist AF-DX384 did not block the carbachol-induced EPSC suppression. These results suggest that NAc MSNs and ChNs are differentially regulated by excitatory projections from the IC and mPFC and that these corticoaccumbal excitatory inputs are modulated by M₁ receptor activation.

Introduction

The nucleus accumbens (NAc), which is a part of the basal ganglia, constitutes the mesolimbic pathway and plays a key role in the information processing of rewards [4]. This NAc function profoundly correlates with pathophysiological states such as drug abuse and addiction. The NAc contains several types of neurons: medium spiny neurons (MSNs), fast-spiking GABAergic neurons (FSNs), and cholinergic interneurons (ChNs) [12, 25, 33]. ChNs, which have large and spindle-shaped somata, account for only ~ 2% of the NAc neuronal population, however, their axons densely project to MSNs and are the main source of acetylcholine in the NAc [38]. The previous study demonstrated that intrinsic acetylcholine released from NAc ChNs reduces the repetitive spike firing frequency of MSNs accompanying depolarization of the resting membrane potential and an increase in input resistance [5]. Zhang and Warren [37] demonstrated that excitatory postsynaptic currents (EPSCs) of MSNs evoked by extracellular electrical stimulation are suppressed and facilitated by the activation of muscarinic and nicotinic receptors, respectively. Overall, activation of ChNs in the NAc suppresses spontaneous spike firing in the NAc of freely moving rats [31]. The cholinergic regulation of neural activities in the NAc is likely to contribute to pathophysiological functions such as cocaine intake [29].

The NAc receives convergent projections from the basolateral amygdala, ventral tegmental area, and midline thalamic nuclei [19]. In addition to these brain regions, there are abundant projections from the cerebral cortex to the NAc, known as corticoaccumbal projections. The insular cortex (IC) and medial prefrontal cortex (mPFC) are principal cortical areas that send their axons to the NAc [7, 19]. Indeed, many studies have demonstrated the functional interactions between the IC/mPFC and NAc. In taste memory formation, IC inputs to the NAc are thought to be a critical factor [21]. Furthermore, the IC-NAc pathway mediates socioemotional behaviors; as a result, this connection is likely to integrate social rewards [22]. On the other hand, glutamatergic inputs from the mPFC to the NAc core are likely to send associative motivationally relevant information [2, 24] and mediate aversion-resistant alcohol addiction [23].

Despite the functional significance of the IC and mPFC in the information processing of the NAc, the fundamental synaptic profiles of IC-NAc and mPFC-NAc connections are still unknown. Considering the differential roles between the IC and mPFC in their physiological functions as described above, IC-NAc and mPFC-NAc synapses may have distinct profiles. In the present study, optogenetics were used to elucidate the synaptic profiles of projections from the IC or the mPFC to the NAc MSNs and ChNs. Furthermore, I examined the cholinergic effects on postsynaptic currents evoked by specific activation of IC or mPFC axon terminals.

Materials and methods

All experiments were performed in accordance with the National Institutes of Health Guide for the Care and Use of Laboratory Animals and were approved by the Institutional Animal Care and Use Committee at Nihon University (approval number, AP20DEN026). All efforts were made to minimize both the number of animals used and their suffering.

Animals

I used adult vesicular GABA transporter (VGAT)-Venus line A transgenic rats (postnatal week > 8; [17, 26] or double-transgenic rats that were obtained by mating a male choline acetyltransferase (ChAT)-tdTomato transgenic rat [36] with a VGAT-Venus transgenic female rat for the experiments using optogenetics. Four- to 5-week-old rats of either sex were anesthetized with 1.5-2.0% isoflurane (Mylan, Tokyo, Japan) and were placed in a stereotaxic frame. The skull surface was exposed, and a small hole was made to insert a needle filled with a 1.0 μ l suspension of adeno-associated virus (AAV) encoding-modified channelrhodopsin-2 (ChR2) fused to mCherry under the control of the human synapsin promoter (AAV5-hSyn-ChR2(H134R)-mCherry; Addgene, Watertown, USA). The virus suspension was delivered at a rate of 75 nl/min into the IC with 2- or 10- μ l syringes (7000 series, Hamilton Company, Reno, USA). The stereotaxic coordinates of the virus injection into the IC of VGAT-Venus rats were 0-0.5 mm posterior to the bregma, 4.5-5.0 mm lateral to the midline, and 4.35 mm in depth. In the case of AAV injection into the IC of the double-transgenic rats, the stereotaxic coordinates were as follows: 0.7 mm anterior to the bregma, 5.0 mm lateral to the midline, and 4.35 mm in depth. The stereotaxic coordinates of the virus injection into the mPFC of double-transgenic rats were 3.0 mm anterior to the bregma, 0.7 mm lateral to the midline, and 2.7 mm in depth. After the injection procedure, the incised skin was sutured with 5-0 silk threads.

Slice preparations

Four to 6 weeks after AAV injection, the animals were used in electrophysiology experiments. The in vitro slice preparation technique was similar to a previously described method [16, 27, 34]. Briefly, rats were deeply anesthetized with isoflurane (5%) and perfused transcardially with the following ice-cold modified artificial cerebrospinal fluid (ACSF): 2.5 KCl, 0.5 CaCl₂, 10 MgSO₄, 1.25 NaH₂PO₄, 2 thiourea, 3 sodium pyruvate, 93 N-methyl-D-glucamine, 20 HEPES, 12 N-acetyl-L-cysteine, 25 D-glucose, 5 L-ascorbic acid, and 30 NaHCO₃ (in mM; pH 7.35-7.40). After decapitation, the brain was rapidly removed and stored in ice-cold modified ACSF. Coronal slices including the NAc and/or IC or mPFC were cut at a thickness of 350 μ m using a microslicer (Linearslicer Pro 7, Dosaka EM, Kyoto, Japan). The slices were incubated at 32 °C for 30 min in a submersion-type holding chamber that contained the modified ACSF. Modified ACSF and normal ACSF were continuously aerated with a

mixture of 95% O₂/5% CO₂. The slices were transferred to a holding chamber with normal ACSF containing 126 NaCl, 3 KCl, 2 MgSO₄, 1.25 NaH₂PO₄, 26 NaHCO₃, 2 CaCl₂, and 10 D-glucose (in mM) at room temperature until used for recording.

Identification of AAV injection site

Coronal slices of the IC and the mPFC were transferred to a recording chamber mounted on a confocal microscope (FV-1000, Olympus, Tokyo, Japan) and examined for AAV injection into the IC or mPFC (Fig. 1). For a part of the experiment, AAV-infected neurons and GABAergic neurons were imaged by alternative laser light application (473 nm and 559 nm), and Kalman filtering was applied. The injection sites were imaged at a resolution of 1600 × 1600 pixels (Fig. 1C).

Whole-cell patch-clamp recording

Slice preparations including the NAc were placed in a recording chamber that was perfused continuously with normal ACSF at a rate of 2.2 ml/min. Thin-wall borosilicate patch electrodes (4-5 MΩ) were pulled on a Flaming-Brown micropipette puller (P-97, Sutter Instruments, Novato, USA). The pipette solution contained the following (E_{Cl} = -65 mV): 135 potassium gluconate, 10 HEPES, 0.5 EGTA, 2 MgCl₂, 2 magnesium ATP, and 0.3 sodium GTP (in mM). The pipette solution had a pH of 7.3 and an osmolality of 300 mOsm. The liquid junction potential of the pipette solution described above was -6 mV. The voltage was not corrected in the present study.

Whole-cell patch-clamp recordings were obtained from NAc neurons using a fluorescence microscope equipped with Nomarski optics (40×, Olympus BX61W1, Tokyo, Japan) and an infrared-sensitive video camera (IR-1000, DAGE-MTI, Michigan City, USA). Recordings were obtained at room temperature. The seal resistance was > 10 GΩ, and only data obtained from electrodes with an access resistance of 6-20 MΩ and < 20% change during recordings were included in this study. The voltage responses were recorded while injecting depolarizing and hyperpolarizing current pulses (300-500 ms) to examine basic membrane properties, including single spike kinetics and repetitive firing patterns and frequency. Electrical signals were recorded with amplifiers (Multiclamp 700B, Molecular Devices, Sunnyvale, USA) and a digitizer (Digidata 1440A, Molecular Devices), and then they were observed online and stored on a computer hard disk using Clampex (pClamp 10, Molecular Devices).

Light stimulation of IC or mPFC axon terminals in the NAc

To activate ChR2 expressed in IC or mPFC neuronal axons, I collimated blue light (470 nm) using an LED system (COPI-A, Thorlabs, Newton, USA) with a water-immersion 40× microscope objective. Light stimulation was applied to the slice preparations with a duration of 3-5 ms, and the light intensity was adjusted to evoke EPSCs with a single peak. To determine whether the light-evoked EPSCs were

monosynaptic or polysynaptic, I applied tetrodotoxin (TTX; Abcam, Cambridge, UK), 4-aminopyridine (4-AP; Nacalai Tesque, Kyoto, Japan), and 6,7-dinitroquinoxaline-2,3-dione (DNQX; Abcam). I also applied carbachol (Abcam), neostigmine (Sigma-Aldrich, St. Louis, USA), atropine (Sigma-Aldrich), pirenzepine (Sigma-Aldrich), gallamine (Fujifilm Wako Pure Chemical, Osaka, Japan), PD102807 (Santa Cruz Biotechnology, Dallas, USA), J104129 (Santa Cruz Biotechnology), and AF-DX384 (Abcam) to examine the effects of cholinergic receptors on light-evoked EPSCs. All drugs were bath-applied to the perfusate.

Date analysis

Clampfit (pClamp 10) was used to analyze electrophysiological data. The average amplitude of the light-evoked EPSCs was obtained from 10-20 consecutive sweeps. The latency of EPSCs was measured from the onset of light stimulation to the onset of the rising phase of EPSCs. The rise time of EPSCs was the time to rise from 20 to 80% of the peak value. The synaptic event threshold was set at the amplitude of 3 times the standard deviation of the baseline. Under the current-clamp condition, depolarizing and hyperpolarizing currents (300-500 ms) were applied to identify the neural subtypes. Input resistance was calculated from the relationship between the injected current intensity (-10 to -40 pA) and the steady-state voltage response (> 250 ms). The repetitive spike firing property (f/I slope) was evaluated by measuring the slope of a least-squares regression line in a plot of the number of spikes versus the amplitude of the injected current.

Typically, recordings made 5 min after drug application were used to quantify the effects of the drug on light-evoked EPSCs. The comparison of the resting membrane potential between MSNs and ChNs was performed using Student's *t*-test. The amplitudes of light-evoked EPSCs were compared using Kruskal-Wallis analysis of variance (ANOVA) on ranks with Dunn's post hoc method or Friedman's repeated measures ANOVA on ranks with Tukey's post hoc test (SigmaStat ver. 4, Systat, San Jose, USA). The latencies and rise time of light-evoked EPSCs were compared using one-way ANOVA with Tukey's post hoc test. The suppression rates of carbachol in combination with gallamine, J104129, PD102807, AF-DX384, or pirenzepine were compared using Welch's *t*-test with Bonferroni correction. The data are presented as the mean \pm the standard error of the mean (SEM). A level of $P < 0.05$ was adopted to indicate significance.

Results

In the present study, whole-cell patch-clamp recordings of MSNs and/or ChNs in the NAc core of rats that received AAV injection into the IC or mPFC were performed (Fig. 1). I primarily used VGAT-Venus transgenic rats (Fig. 1Ca), and ChN recordings were performed using double-transgenic rats to identify ChNs in the NAc (Fig. 1Cb). I elucidated the functional properties of the projections from the IC or mPFC to the NAc core and examined the cholinergic effects of these projections on the NAc core.

Cell identification

The NAc contains at least 3 types of neurons, i.e., MSNs, FSNs, and ChNs [12, 25, 33], and these neurons have distinct functional roles. I first identified MSNs by their anatomical profiles. MSNs have small somata with Venus fluorescent proteins (Fig. 1C) [5, 12, 33]. Then, I applied depolarizing long-current pulse injections around the spike threshold to examine the characteristic depolarizing potential in MSNs: a long-lasting ramp depolarization before spike initiation (Fig. 2A) [5, 12, 33]. The resting membrane potential, input resistance, and f/I slope of NAc MSNs in the present study were -72.2 ± 0.8 mV, 225.4 ± 18.1 M Ω ($n = 85$), and 0.26 ± 0.02 Hz/pA ($n = 84$), respectively. These profiles almost matched the previous results of NAc MSNs [5, 12, 33].

To record from ChNs, I used double-transgenic rats, in which GABAergic neurons and ChNs were labeled by the green fluorescent protein Venus and the red fluorescent protein tdTomato, respectively (Fig. 1Cb). The resting membrane potential of ChNs (-61.8 ± 0.7 mV, $n = 65$) was more depolarized than that of MSNs described above ($P < 0.001$, Student's t -test). ChNs often showed sag and rebound spikes in response to long hyperpolarizing current pulse injections (Fig. 2B). Input resistance and f/I slope of ChNs were 293.8 ± 23.8 M Ω ($n = 60$), and 0.23 ± 0.02 Hz/pA ($n = 64$), respectively. Both of these profiles look to be larger than the previous results of NAc ChNs [5], possibly because of differences in the age and strain of the rat.

Another cell type in the NAc is the FSN, which was Venus-positive but tdTomato-negative and showed high-frequency repetitive spike firing with little spike adaptation (Fig. 2C). I excluded FSNs from the following analyses.

Properties of light-evoked postsynaptic currents in IC-NAc MSN synapses

After cell identification, blue light (473 nm) stimulation was applied to the slice preparation. Figure 3A shows typical examples of light-evoked EPSPs/EPSCs recorded from the MSN in rats that received AAV injection into the IC. Under voltage-clamp conditions (holding potential = -60 mV), phase-locked inward currents were evoked in response to light stimulation (Fig. 3B). The latency of the response from the onset of light stimulation was 6.0 ± 0.2 ms ($n = 58$). The amplitude and 20-80% rise

time were 129.2 ± 24.4 pA and 2.4 ± 0.1 ms ($n = 65$), respectively. Under current-clamp conditions, blue light application induced depolarizing potentials (Fig. 3C). At depolarized resting membrane potentials by application of direct current, blue light stimulation sometimes induced action potentials (Fig. 3C arrowhead).

Some neurons (23.5%, 20/85) produced light-evoked EPSCs with subsequent outward currents (Fig. 3D arrows). The outward currents were diminished by bicuculline, suggesting that these outward currents were mediated via GABA_A receptors (data not shown). Indeed, recordings under current-clamp conditions from neurons showing outward currents demonstrated light-evoked EPSPs followed by hyperpolarized potentials (Fig. 3E). I did not observe light-evoked IPSCs without preceding EPSCs: all light-evoked IPSCs were observed immediately after light evoked EPSCs.

Although approximately one quarter of the evaluated neurons exhibited light-evoked IPSCs, the principal light-evoked currents were EPSCs. Therefore, light-evoked EPSCs were the focus of the following analyses.

Monosynaptic EPSCs from the IC to NAc MSNs

The application of TTX, a voltage-gated Na⁺ channel blocker, with 4-AP, a blocker of K⁺ channels, is an appropriate approach to distinguish whether ChR2-evoked EPSCs are monosynaptic or polysynaptic [6]: TTX-induced blockade of voltage-gated Na⁺ channels diminishes action potentials, and 4-AP induces greater depolarization by cation influx via ChR2, which causes Ca²⁺ influx sufficient to induce glutamate release.

Bath application of 1 μM TTX, a voltage-gated Na⁺ channel blocker, abolished light-evoked EPSCs (69.1 ± 23.6 pA for control conditions and 2.5 ± 0.5 pA with TTX, $n = 8$; $P < 0.01$, Friedman's repeated measures ANOVA on ranks with Tukey's post hoc test; Fig. 4). The inward currents were recovered by 1 mM 4-AP, a K⁺ channel blocker that potentiates neurotransmitter release from presynaptic terminals, with TTX (36.0 ± 9.6 pA with TTX and 4-AP, $n = 8$; $P < 0.05$, Friedman's repeated measures ANOVA on ranks with Tukey's post hoc test; Fig. 4), indicating that the inward currents were EPSCs mediated by glutamatergic AMPA receptors.

NAc ChNs receive only faint excitatory inputs from the IC

The NAc contains ChNs, which make up ~2% of NAc neurons [38]. I next examined the IC inputs to NAc ChNs using double-transgenic rats that expressed a fluorescent protein, tdTomato, in ChNs (Fig. 5A). To avoid the argument that the difference in light-evoked EPSC amplitude between MSNs and ChNs arises from the slice condition, I performed paired whole-cell recordings from MSNs and neighboring ChNs in the same slice preparations.

Figure 5B, C shows a typical example of a paired whole-cell patch-clamp recording from an MSN and a ChN. Light stimulation evoked EPSCs in the MSN but not in the ChN. Only 28.6% (8/28)

of ChNs from AAV-injected rats in the IC showed detectable light-evoked EPSCs, and the other ChNs showed no response to the light stimuli of IC axons (Fig. 5G). Overall, light-evoked EPSCs in ChNs (2.6 ± 0.9 pA, $n = 28$), which included ChNs without light-evoked EPSCs, were significantly smaller than those of MSNs that were simultaneously recorded (213.2 ± 49.6 pA, $n = 28$; $P < 0.001$, Kruskal-Wallis ANOVA on ranks with Dunn's post hoc method; Fig. 5G). I did not quantify the rise time of EPSCs obtained from ChNs of AAV-injected rats in the IC because of their small amplitude. These results suggest that ChNs receive much fewer IC projections than MSNs.

Both MSNs and ChNs receive excitatory inputs from the mPFC

In addition to the IC, the mPFC is another principal source of cerebrocortical projections to the NAc [7, 19]. Taking into account their different physiological functions, there is a possibility that the mPFC differentially regulates NAc neurons from the IC. To test this possibility, I next examined the light-evoked excitatory inputs from the mPFC to NAc MSNs and ChNs using double-transgenic rats that received AAV injection into the mPFC (Fig. 5D-F).

In the recordings from MSNs of AAV-injected rats in the mPFC, the light stimulation evoked EPSCs, and the amplitude of light-evoked EPSCs was 147.1 ± 32.2 pA ($n = 34$), which was comparable to that obtained from the AAV-injected rats in the IC described above ($P = 1.0$; Kruskal-Wallis ANOVA on ranks with Dunn's post hoc method; Fig. 5G). The latency of the light-evoked EPSCs of MSNs in AAV-injected rats in the mPFC (5.3 ± 0.3 ms, $n = 33$) was also comparable to that in AAV-injected rats in the IC (4.9 ± 0.2 ms, $n = 27$; $P = 0.051$; one-way ANOVA; Fig. 5H). The 20-80% rise time 3.0 ± 0.2 ms ($n = 27$) was comparable to that obtained from MSNs of AAV-injected rats in the IC ($P = 0.126$, one-way ANOVA; Fig. 5I). In addition, the light-evoked EPSCs of MSNs in AAV-injected rats in the mPFC were diminished by $1 \mu\text{M}$ TTX and rescued by 1 mM 4-AP, as shown in Fig. 5E. These results suggest the monosynaptic activation of NAc MSNs by mPFC axons, similar to that by IC axons.

In contrast to the similarity between the light-evoked EPSCs recorded from MSNs of AAV-injected rats in the IC and those in the mPFC, ChNs showed differential properties in their light-evoked EPSCs when comparing the IC and mPFC. Most ChNs of AAV-injected rats in the mPFC showed light-evoked EPSCs (Fig. 5F), and only 3% (1/34) of ChNs in those rats showed no response to light stimuli. The mean amplitude was 15.3 ± 2.1 pA ($n = 33$), which was smaller than that of MSNs ($P < 0.001$; Kruskal-Wallis ANOVA on ranks with Dunn's post hoc method; Fig. 5G) and larger than that of the ChNs of AAV-injected rats in the IC ($P < 0.01$; Kruskal-Wallis ANOVA on ranks with Dunn's post hoc method; Fig. 5G). The latency of the light-evoked EPSCs of ChNs in AAV-injected rats in the mPFC was 5.9 ± 0.3 ms ($n = 33$). These latencies of ChNs in AAV-injected rats in the IC and mPFC were comparable to those of MSNs ($P = 0.051$, one-way ANOVA; Fig. 5H). On the other hand, the 20-80% rise time of the light-evoked EPSCs of ChNs in AAV-injected rats in the mPFC was 3.6 ± 0.3 ms ($n = 33$), which was comparable to that of MSNs in AAV-injected rats in the mPFC ($P = 0.07$)

but longer than that of MSNs in AAV-injected rats in the IC ($P < 0.001$, one-way ANOVA with Tukey's post hoc test; Fig. 5I). This may be due to the smaller EPSC amplitude of ChNs than that of MSNs.

These results suggest that MSNs receive excitatory inputs from the mPFC comparable to those from the IC, whereas ChNs receive cortical projections from the mPFC but not from the IC.

Cholinergic modulation of light-induced EPSCs

Acetylcholine is a key modulator that changes the neural activities of NAc neurons [3, 5, 33], however, little information is available in terms of corticoaccumbal excitatory inputs. Thus, I next examined the cholinergic effect on light-evoked EPSCs in MSNs of the NAc.

A representative example of the effect of carbachol on light-evoked EPSCs recorded from MSNs that received an AAV-infected projection from the IC is shown in Fig. 6A and B. Carbachol (10 μM), a cholinergic agonist, effectively suppressed the amplitude of light-evoked EPSCs. In sum, 10 μM carbachol suppressed light-induced EPSCs: 57.8 ± 16.3 pA in the control condition and 37.4 ± 14.3 pA during carbachol application ($n = 15$; $P < 0.01$, Friedman's repeated measures ANOVA on ranks with Tukey's post hoc test).

Similar to the IC projection to NAc MSNs, light-evoked EPSCs recorded from MSNs that received an AAV-infected projection from the mPFC were suppressed by 10 μM carbachol from 139.0 ± 43.7 pA to 60.2 ± 18.3 pA ($n = 7$; $P < 0.05$, Friedman's repeated measures ANOVA on ranks with Tukey's post hoc test). Light-evoked EPSCs recorded from ChNs that received an AAV-infected projection from the mPFC were also suppressed by 10 μM carbachol from 30.2 ± 11.2 pA to 20.0 ± 7.2 pA ($n = 8$; $P < 0.01$, Friedman's repeated measures ANOVA on ranks with Tukey's post hoc test).

These results suggest that cholinergic receptor activation consistently suppresses EPSCs evoked by cortical fiber activation in both MSNs and ChNs.

M₁ receptor-mediated suppression of light-induced EPSCs

To explore which type of cholinergic receptors contribute to carbachol-induced suppression of light-evoked EPSCs, I examined the effects of atropine, a nonselective muscarinic antagonist, and pirenzepine, an M₁ receptor antagonist.

The suppressive effect of carbachol on light-evoked EPSCs recorded from MSNs that received an AAV projection from the IC was rapidly recovered by a co-application of 20 μM atropine: 54.4 ± 23.1 pA in the control, 27.5 ± 12.8 pA with carbachol, and 59.1 ± 29.1 pA during carbachol and atropine application ($n = 7$; $P < 0.01-0.05$, Friedman's repeated measures ANOVA on ranks with Tukey's post hoc test; Fig. 6E). The amplitudes of light-evoked EPSCs in the control and after application of atropine were comparable ($P = 0.961$, Friedman's repeated measures ANOVA on ranks with Tukey's post hoc test; Fig. 6E).

The effect of atropine was mimicked by 10 μM pirenzepine, as shown in Fig. 6C, D and Fig.

7. Since pirenzepine induced a recovery of light-evoked EPSCs from suppression by carbachol both in MSNs recorded from rats with AAV injection into the IC and in the mPFC, I combined the results of pirenzepine obtained from both MSNs: 109.1 ± 28.7 pA in the control, 40.3 ± 11.7 pA with carbachol, and 88.3 ± 21.3 pA during co-application of carbachol and pirenzepine ($n = 13$; $P < 0.001-0.01$, Friedman's repeated measures ANOVA on ranks with Tukey's post hoc test; Fig. 6F). The amplitudes of light-evoked EPSCs in the control and after application of pirenzepine were comparable ($P = 0.181$, Friedman's repeated measures ANOVA on ranks with Tukey's post hoc test; Fig. 6F).

I also tested the effect of pirenzepine on light-evoked EPSCs recorded from ChNs in rats with AAV injection into the mPFC and found a similar effect of pirenzepine on light-evoked EPSCs: 30.2 ± 10.5 pA in the control, 20.0 ± 6.7 pA with carbachol, and 30.9 ± 12.7 pA during carbachol and pirenzepine application ($n = 8$; $P < 0.01-0.05$, Friedman's repeated measures ANOVA on ranks with Tukey's post hoc test; Fig. 6G). The amplitudes of light-evoked EPSCs in the control and after application of pirenzepine were comparable ($P = 0.871$, Friedman's repeated measures ANOVA on ranks with Tukey's post hoc test; Fig. 6G).

In addition, a representative example of the effect of neostigmine on light-evoked EPSCs recorded from MSNs that received an AAV-infected projection from the IC is shown in Fig. 7 under depolarizing current pulse injection to ChN. Neostigmine ($100 \mu\text{M}$), a cholinesterase inhibitor, effectively suppressed the amplitude of light-evoked EPSCs. In sum, $100 \mu\text{M}$ neostigmine suppressed light-induced EPSCs from 472.8 ± 117.1 pA to 315.0 ± 101.0 pA ($n = 6$; $P < 0.05$, paired t -test). Also, pirenzepine rescued the suppression of EPSCs by neostigmine from 315.0 ± 101.0 pA to 443.9 ± 120.0 pA in MSNs from rats with AAV injection into the IC ($n = 6$; $P < 0.05$, paired t -test).

These results suggest that glutamatergic synaptic transmission from the IC/mPFC to NAc MSNs/ChNs is suppressed by activation of M_1 receptors.

M₂, M₃, and M₄ receptor antagonists have little effect on carbachol-mediated suppression of light-induced EPSCs

Although pirenzepine is applied as a selective antagonist for M_1 receptors, it has been reported that pirenzepine has low but significant affinity for M_2 , M_3 , and M_4 [30]. Furthermore, M_2/M_4 receptors are expressed in presynaptic neurons [13]. Therefore, there is the possibility that pirenzepine might block carbachol-mediated suppression of light-induced EPSCs not only via M_1 but also via $M_2/M_3/M_4$ receptors. To explore this possibility, I examined the effects of preapplication of a negative M_2 allosteric modulators gallamine, M_3 receptor antagonist J104129, M_4 receptor antagonist PD102807, or M_2/M_4 receptor antagonist AF-DX384 on carbachol-mediated suppression of light-induced EPSCs obtained from MSNs of AAV-injected rats in the IC.

Under application of gallamine ($200 \mu\text{M}$), J104129 (500 nM), PD102807 ($5 \mu\text{M}$), or AF-DX384 ($2 \mu\text{M}$), carbachol ($10 \mu\text{M}$) suppressed light-evoked EPSCs as shown in Fig. 8C-F. The

suppression rate of carbachol (EPSC amplitude during carbachol application/EPSC amplitude without carbachol) was $56.2 \pm 4.5\%$ ($n = 33$). Under application of gallamine, J104129, PD102807, and AF-DX384, carbachol suppressed the amplitude of EPSCs to $70.0 \pm 4.4\%$ ($n = 10$), $62.4 \pm 3.7\%$ ($n = 13$), $62.2 \pm 7.1\%$ ($n = 10$), and $65.6 \pm 2.7\%$ ($n = 19$), respectively, which were comparable to the suppression rate of carbachol without an antagonist ($P = 0.272 - 1$, Welch's *t*-test with Bonferroni correction; Fig. 7G). On the other hand, preapplication of 10 μM pirenzepine significantly blocked carbachol-mediate suppression of light-induced EPSCs ($90.0 \pm 2.8\%$, $n = 19$; $P < 0.001$, Welch's *t*-test with Bonferroni correction; Fig. 8A, G). I also tested preapplication of 2 μM pirenzepine, and found a significant blockade of carbachol-mediated suppression of light-induced EPSCs ($96.5 \pm 2.1\%$, $n = 10$; $P < 0.001$, Welch's *t*-test with Bonferroni correction; Fig. 8A, G).

These results support that carbachol suppresses light-induced EPSCs via M_1 receptors.

Discussion

The significance of identifying the source of EPSCs and recorded neurons in the NAc

It has been demonstrated that projection neurons to other cortical areas or to areas outside of the cerebral cortex are layer V pyramidal neurons [10]. Similar to this principle found in other cortical areas, my results demonstrated that projection neurons from the IC to the NAc were glutamatergic and induced EPSCs in MSNs. In addition to inputs from IC neurons, NAc MSNs receive glutamatergic inputs from other brain regions, such as the PFC, amygdala, ventral tegmental area, and midline thalamic nuclei [19]. Muscarinic M₁/M₄ receptor agonists suppress evoked EPSCs in a presynaptic manner by causing a decrease in the release probability of glutamate from presynaptic terminals [37]. However, extracellular electrical stimulation activates glutamatergic axons from the various brain regions described above and other fibers, such as GABAergic, cholinergic, and dopaminergic axons. Extracellular electrical stimulation may lead to divergent effects on EPSCs for each glutamatergic input. I cannot deny the possibility that some glutamatergic inputs are enhanced, whereas other glutamatergic inputs are slightly decreased, and overall, the cholinergic effects are suppressive. Therefore, the present results confirm previous findings and extend them to demonstrate that glutamatergic inputs from the IC to the NAc are indeed suppressed via M₁ receptors. This finding is critical because each glutamatergic input has its own functional roles.

Differential activation patterns of NAc ChNs by the IC and mPFC

The previous study involved multiple whole-cell patch-clamp recordings from ChNs and adjacent MSNs, and the results suggested the cholinergic modulation of MSN activity by adjacent ChNs [5]. Thus, NAc ChNs are also likely to mediate cholinergic suppression of EPSCs via M₁ receptors. The principal origins of corticoaccumbal projections are the IC and PFC, including the mPFC and entorhinal cortex [7, 19]. These cortical areas have their own physiological functions; for example, the IC-NAc connections process taste memory formation [21] and socioemotional behaviors [22], while the mPFC plays a critical role in higher brain functions, including associative motivation [2, 24], and mediates aversion-resistant alcohol addiction [23]. Therefore, it is reasonable to postulate that corticoaccumbal projections differentially activate NAc neurons, which would generate distinct functions depending on the cortical area. The present finding of mPFC- but not IC-dependent activation of ChNs may represent a functional difference between the IC and mPFC. Activation of NAc MSNs by the IC might be weakened by simultaneous activation of the mPFC, which drives NAc ChNs and, as a result, suppresses EPSCs in IC-NAc MSN connections.

Inhibitory inputs to NAc MSNs

The NAc contains several types of neurons: MSNs, FSNs, and ChNs [12, 25, 33]. MSNs are the

principal neurons that make up approximately 95% of NAc neurons and are considered to play a pivotal role in limbic information processing because MSNs send their GABAergic axons to the ventral pallidum. On the other hand, FSNs are interneurons that induce large IPSCs in adjacent neurons, including MSNs [12]. Therefore, the functional roles of MSNs and FSNs are opposing: excitatory inputs to MSNs facilitate GABAergic outputs from the NAc to the ventral pallidum, and excitatory inputs to FSNs are likely to result in the inhibition of MSNs and a decrease in GABAergic outputs from the NAc. The present study demonstrated abundant glutamatergic inputs from the IC and mPFC to NAc MSNs. In addition, some MSNs receive GABAergic inputs in combination with glutamatergic inputs, suggesting two possibilities. First, activation of MSNs by IC excitatory inputs induces the inhibition of adjacent MSNs via their axon collaterals [12, 33]. Second, excitatory projections from the IC terminate not only on MSNs but also on FSNs, which potently suppress MSN activity [12]. Future studies should explore these possibilities.

Functional implications

Anatomical evidence shows that IC subdivisions play different physiological roles: the most rostral part of the IC, occupied by the agranular IC, plays a role in nociception [9], the dysgranular IC and granular IC around the middle cerebral artery process gustatory information [32], and the caudally adjacent IC receives somatosensory information in the oral region [8, 18]. Therefore, the cholinergic suppression of IC-NAc MSN excitatory synapses presented in this study may have a variety of functions in terms of multisensory information processing. Although only a few behavioral studies have demonstrated the functional coupling between the IC and the NAc, Ramírez-Lugo et al. demonstrated the contribution of the IC-NAc pathway to taste memory formation, in which cholinergic systems, including the nucleus basalis magnocellularis, play a pivotal role [21]. The content of acetylcholine in the NAc is increased by saccharin administration into the oral cavity [14]. Therefore, the present result of the cholinergic attenuation of EPSCs in the IC-NAc pathway may indicate a facilitative role in taste memory formation.

Another aspect of the corticoaccumbal projection is related to reward. Chemogenetic manipulations of the IC-NAc pathway in adult rats demonstrated that stimulation of this pathway increases social exploration in stressed juvenile rats, whereas inhibition of this pathway blocks the preference of stressed juvenile rats [22]. Therefore, cholinergic suppression of EPSCs in the IC-NAc pathway may contribute to the regulation of social reward. Moreover, it was reported that excitatory inputs from the mPFC and IC to the NAc core promote quinine-resistant or footshock-resistant operant two-bottle-choice alcohol intake [23]. Therefore, the cholinergic suppression of corticoaccumbal excitation may play a role in alcohol addiction relief. This process may involve dopamine release in the NAc, which is evoked by glutamatergic inputs from the mPFC and acetylcholine from ChNs [15]. Simultaneous activation of the mPFC in addition to the IC may suppress these possible physiological/

pathophysiological functions.

Acknowledgments

I am grateful to Prof. Tetsuo Shirakawa for the opportunity to perform this study, Prof. Masayuki Kobayashi, Assist. Profs. Yuka Nakaya, Kiyofumi Yamamoto, and Dr. Kohei Kitano for their instructions of this study, and colleagues in Department of Pharmacology for their technical advice and assistance.

References

1. Arguello AA, Wang R, Lyons CM, Higginbotham JA, Hodges MA, Fuchs RA (2017) Role of the agranular insular cortex in contextual control over cocaine-seeking behavior in rats. *Psychopharmacology* 234:2431-2441
2. Brog JS, Salyapongse A, Deutch AY, Zahm DS (1993) The patterns of afferent innervation of the core and shell in the “accumbens” part of the rat ventral striatum: immunohistochemical detection of retrogradely transported fluoro-gold. *J Comp Neurol* 338:255-278
3. de Rover M, Lodder JC, Kits KS, Schofelmeer AN, Brussaard AB (2002) Cholinergic modulation of nucleus accumbens medium spiny neurons. *Eur J Neurosci* 16:2279-2290
4. Di Chiara G (2002) Nucleus accumbens shell and core dopamine: differential role in behavior and addiction. *Behav Brain Res* 137:75-114
5. Ebihara K, Yamamoto K, Ueda K, Koshikawa N, Kobayashi M (2013) ChNs suppress action potential initiation of medium spiny neurons in rat nucleus accumbens shell. *Neuroscience* 236:332–344
6. Felix-Ortiz AC, Beyeler A, Seo C, Leppla CA, Wildes CP, Tye KM (2013) BLA to vHPC inputs modulate anxiety-related behaviors. *Neuron* 79:658-664
7. Groenewegen HJ, Room P, Witter MP, Lohman AH (1982) Cortical afferents of the nucleus accumbens in the cat, studied with anterograde and retrograde transport techniques. *Neuroscience* 7:977-996
8. Horinuki E, Shinoda M, Shimizu N, Koshikawa N, Kobayashi M (2015) Orthodontic force facilitates cortical responses to periodontal stimulation. *J Dent Res* 94:1158-1166
9. Jasmin L, Rabkin SD, Granato A, Boudah A, Ohara PT (2003) Analgesia and hyperalgesia from GABA-mediated modulation of the cerebral cortex. *Nature* 424:316-320
10. Kawaguchi Y, Otsuka T, Morishima M, Ushimaru M, Kubota Y (2019) Control of excitatory hierarchical circuits by parvalbumin-FS basket cells in layer 5 of the frontal cortex: insights for cortical oscillations. *J Neurophysiol* 121:2222-2236
11. Kobayashi M, Cui Y, Sako T, Sasabe T, Mizoguchi N, Yamamoto K, Wada Y, Kataoka Y, Koshikawa N (2013) Functional neuroimaging of aversive taste-related areas in the alert rat revealed by positron emission tomography. *J Neurosci Res* 91:1363-1370
12. Kohnomi S, Koshikawa N, Kobayashi M (2012) D2-like dopamine receptors differentially regulate unitary IPSCs depending on presynaptic GABAergic neuron subtypes in rat nucleus accumbens shell. *J Neurophysiol* 107:692-703
13. Kubista H, Kosenburger K, Mahlknecht P, Drobny H, Boehm S (2009) Inhibition of transmitter release from rat sympathetic neurons via presynaptic M₁ muscarinic acetylcholine receptors. *Br J Pharmacol* 156:1342-1352

14. Mark GP, Weinberg JB, Rada PV, Hoebel BG (1995) Extracellular acetylcholine is increased in the nucleus accumbens following the presentation of an aversively conditioned taste stimulus. *Brain Res* 688:184-188
15. Mateo Y, Johnson KA, Covey DP, Atwood BK, Wang HL, Zhang S, Gildish I, Cachope R, Bellocchio L, Guzman M, Morales M, Cheer JF, Lovinger DM (2017) Endocannabinoid actions on cortical terminals orchestrate local modulation of dopamine release in the nucleus accumbens. *Neuron* 96:1112-1126
16. Murayama S, Yamamoto K, Fujita S, Takei H, Inui T, Ogiso B, Kobayashi M (2019) Extracellular glucose-dependent IPSC enhancement by leptin in fast-spiking to pyramidal neuron connections via JAK2-PI3K pathway in the rat insular cortex. *Neuropharmacology* 149:133-148
17. Nagai T, Ibata K, Park ES, Kubota M, Mikoshiba K, Miyawaki A (2002) A variant of yellow fluorescent protein with fast and efficient maturation for cell-biological applications. *Nat Biotechnol* 20:87-90
18. Nakamura H, Kato R, Shirakawa T, Koshikawa N, Kobayashi M (2015) Spatiotemporal profiles of dental pulp nociception in rat cerebral cortex: an optical imaging study. *J Comp Neurol* 523:1162-1174
19. Phillipson OT, Griffiths AC (1985) The topographic order of inputs to nucleus accumbens in the rat. *Neuroscience* 16:275-296
20. Pushparaj A, Hamani C, Yu W, Shin DS, Kang B, Nobrega JN, Le Foll B (2013) Electrical stimulation of the insular region attenuates nicotine-taking and nicotine-seeking behaviors. *Neuropsychopharmacology* 38:690-698
21. Ramírez-Lugo L, Núñez-Jaramillo L, Bermúdez-Rattoni F (2007) Taste memory formation: role of nucleus accumbens. *Chem Senses* 32:93-97
22. Rogers-Carter MM, Djerdjaj A, Gribbons KB, Varela JA, Christianson JP (2019) Insular cortex projections to nucleus accumbens core mediate social approach to stressed juvenile rats. *J Neurosci* 39:8717-8729
23. Seif T, Chang SJ, Simms JA, Gibb SL, Dadgar J, Chen BT, Harvey BK, Ron D, Messing RO, Bonci A, Hopf FW (2013) Cortical activation of accumbens hyperpolarization-active NMDARs mediates aversion-resistant alcohol intake. *Nat Neurosci* 16:1094-1100
24. Sesack SR, Deutch AY, Roth RH, Bunney BS (1989) Topographical organization of the efferent projections of the medial prefrontal cortex in the rat: an anterograde tract-tracing study with *Phaseolus vulgaris* leucoagglutinin. *J Comp Neurol* 290:213-242
25. Taverna S, Canciani B, Pennartz CM (2007) Membrane properties and synaptic connectivity of fast-spiking interneurons in rat ventral striatum. *Brain Res* 1152:49-56
26. Uematsu M, Hirai Y, Karube F, Ebihara S, Kato M, Abe K, Obata K, Yoshida S, Hirabayashi M, Yanagawa Y, Kawaguchi Y (2008) Quantitative chemical composition of cortical GABAergic

- neurons revealed in transgenic venus-expressing rats. *Cereb Cortex* 18:315-330
27. Usui M, Kaneko K, Oi Y, Kobayashi M (2019) Orexin facilitates GABAergic IPSCs via postsynaptic OX1 receptors coupling to the intracellular PKC signalling cascade in the rat cerebral cortex. *Neuropharmacology* 149:97-112
 28. Venniro M, Zhang M, Caprioli D, Hoots JK, Golden SA, Heins C, Morales M, Epstein DH, Shaham Y (2018) Volitional social interaction prevents drug addiction in rat models. *Nat Neurosci* 21:1520-1529
 29. Weikop P, Jensen KL, Thomsen M (2020) Effects of muscarinic M1 receptor stimulation on reinforcing and neurochemical effects of cocaine in rats. *Neuropsychopharmacology* 45:1994-2002
 30. Wess J, Lambrecht G, Mutschler E, Brann MR, Dörje F (1991) Selectivity profile of the novel muscarinic antagonist UH-AH 37 determined by the use of cloned receptors and isolated tissue preparations. *Br J Pharmacol* 102:246-250
 31. Witten IB, Lin SC, Brodsky M, Prakash R, Diester I, Anikeeva P, Gradinaru V, Ramakrishnan C, Deisseroth K (2010) ChNs control local circuit activity and cocaine conditioning. *Science* 330:1677-1681
 32. Yamamoto T (1984) Taste responses of cortical neurons. *Prog Neurobiol* 23:273-315
 33. Yamamoto K, Ebihara K, Koshikawa N, Kobayashi M (2013) Reciprocal regulation of inhibitory synaptic transmission by nicotinic and muscarinic receptors in rat nucleus accumbens shell. *J Physiol* 591:5745-5763
 34. Yamamoto K, Kobayashi M (2018) Opposite roles in short-term plasticity for N-type and P/Q-type voltage-dependent calcium channels in GABAergic neuronal connections in the rat cerebral cortex. *J Neurosci* 38:9814-9828
 35. Yasui Y, Breder CD, Saper CB, Cechetto DF (1991) Autonomic responses and efferent pathways from the insular cortex in the rat. *J Comp Neurol* 303:355-374
 36. Zhang Y, Kaneko R, Yanagawa Y, Saito Y (2014) The vestibulo-and prepositus-cerebellar cholinergic neurons of a ChAT-tdTomato transgenic rat exhibit heterogeneous firing properties and the expression of various neurotransmitter receptors. *Eur J Neurosci* 39:1294-1313
 37. Zhang L, Warren RA (2002) Muscarinic and nicotinic presynaptic modulation of EPSCs in the nucleus accumbens during postnatal development. *J Neurophysiol* 88:3315-3330
 38. Zhou FM, Wilson C, Dani JA (2003) Muscarinic and nicotinic cholinergic mechanisms in the mesostriatal dopamine systems. *Neuroscientist* 9:23-36

Figures

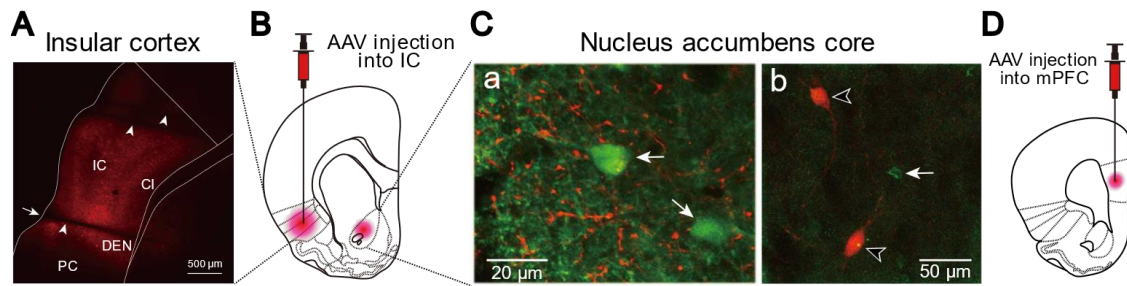


Fig. 1. *A*, Confocal images of adeno-associated virus serotype 5 (AAV5-hSyn-ChR2(H134R)-mCherry; AAV) expression in the insular cortex (IC). The rhinal fissure is indicated by an arrow. Arrowheads indicate the threads used to fix the slice (Cl, claustrum; PC, piriform cortex; DEN, endopiriform nucleus). *B*, A schematic of a brain slice preparation receiving an injection of AAV into the IC. *Ca*, Axons labeled with a fluorescent protein, mCherry from the IC (red) and GABAergic neurons labeled with Venus protein (green; arrows) observed in the nucleus accumbens (NAc). *Cb*, Cholinergic neurons (ChNs; open arrowheads) were easily identified in the double transgenic rat by their fluorescent protein, tdTomato. *D*, A schematic of a brain slice preparation receiving an injection of AAV into the medial prefrontal cortex (mPFC).

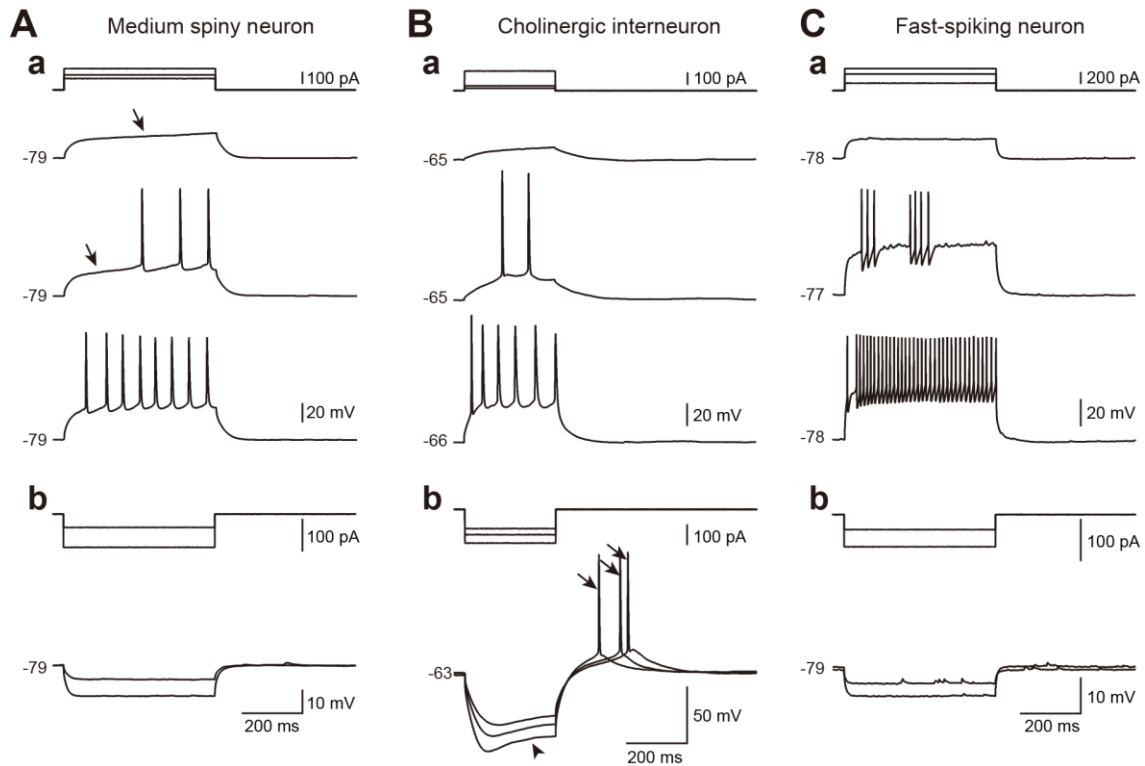


Fig. 2. Classification of neurons in the NAc. **Aa**, Firing properties of a medium spiny neuron (MSN) responding to a depolarizing current pulse injection (top). Lower traces represent voltage responses of the MSN. Arrows indicate a characteristic ramp depolarizing potential under the spike threshold and temporal lags before repetitive spike firing. **Ab**, The voltage responses to the hyperpolarizing current pulse injection obtained from the same MSN shown in **Aa**. **Ba**, Firing properties of a cholinergic interneuron (ChN) responding to a depolarizing current pulse injection (top). **Bb**, The voltage responses to the hyperpolarizing current pulse injection obtained from the same ChN shown in **Ba**. Note that the initial membrane hyperpolarization is followed by the characteristic depolarizing sag (arrowhead) and rebound action potentials (arrows). **Ca**, Firing properties of a fast-spiking neuron (FSN) responding to a depolarizing current pulse injection (top). Note the large afterhyperpolarization and extremely high repetitive firing frequency. **Cb**, The voltage responses to the hyperpolarizing current pulse injection obtained from the same FSN shown in **Ca**. The resting potential is shown on the left of each voltage trace.

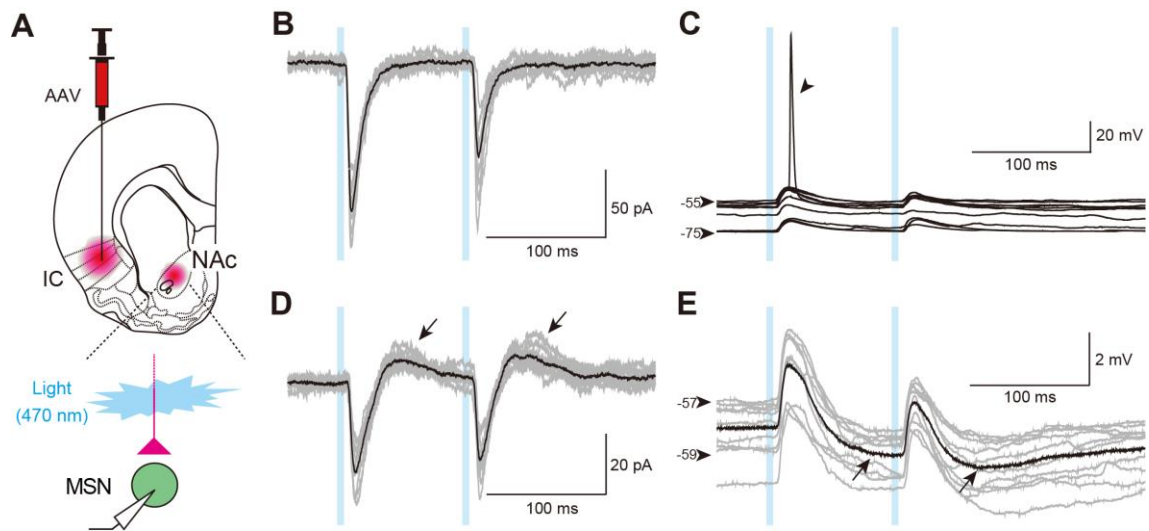


Fig. 3. Light-evoked inward and outward currents/potentials recorded from MSNs in the NAc. **A**, A schematic of a brain slice preparation receiving an injection of AAV into the IC. Whole-cell patch-clamp recording was performed from NAc MSNs. **B**, An example of an MSN showing light-evoked inward currents (EPSCs) under voltage-clamp conditions (holding potential = -60 mV). Ten consecutive current responses to paired blue light stimulation (top) in the control (gray). A thick black trace is obtained by averaging these ten traces. **C**, Light-evoked EPSPs responding to light stimulation under the current-clamp condition in the same neuron shown in **B**. Note an action potential (arrowhead) at the depolarized resting membrane potential induced by a positive current injection. **D**, An example of an MSN showing outward currents after EPSCs (arrows). **E**, Light-evoked IPSPs (arrows) are observed under the current-clamp condition in the same MSN shown in **D**. Vertical blue stripes in **B-E** indicate the period of blue light application to the slice preparation.

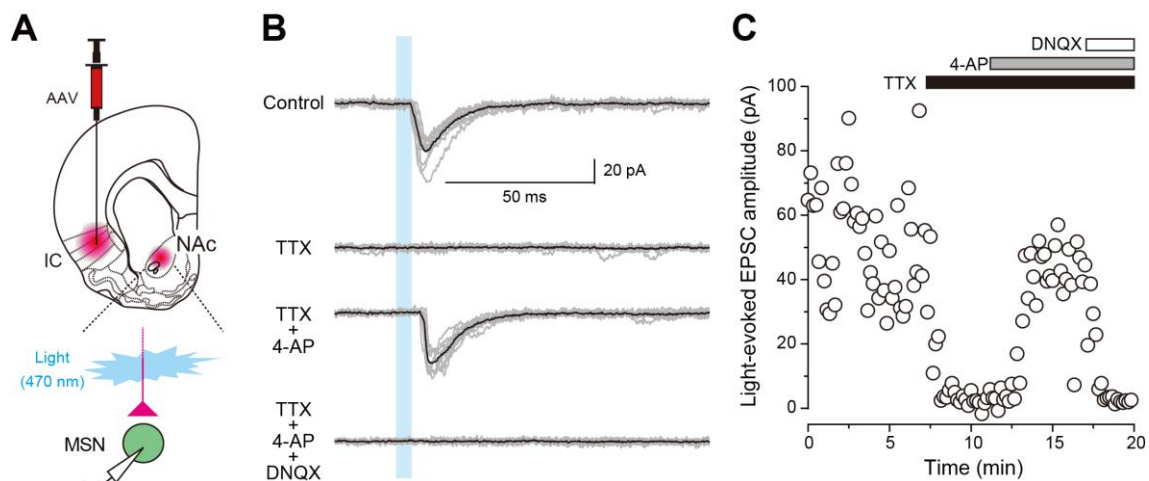


Fig. 4. Effects of tetrodotoxin (TTX), 4-aminopyridine (4-AP), and 6,7-dinitroquinoxaline-2,3-dione (DNQX) on light-evoked EPSCs recorded from an MSN. **A**, A schematic of whole-cell patch-clamp recording from an NAc MSN receiving AAV-infected IC axons. **B**, Ten consecutive current responses (gray) with their averaged trace (black) to paired blue light stimulation (blue stripe) in the control during the application of 1 μ M tetrodotoxin (TTX), co-application of TTX and 1 mM 4-AP (TTX + 4-AP), and co-application of TTX, 4-AP, and 40 μ M DNQX (TTX + 4-AP + DNQX). Note that TTX diminishes light-evoked EPSCs, which are recovered by the co-application of 4-AP. The decline in light-evoked EPSCs by DNQX treatment indicates that light-evoked EPSCs are mediated via AMPA receptors. The holding potential was set at -60 mV. **C**, The time course of the amplitude of light-evoked EPSCs before and during drug application.

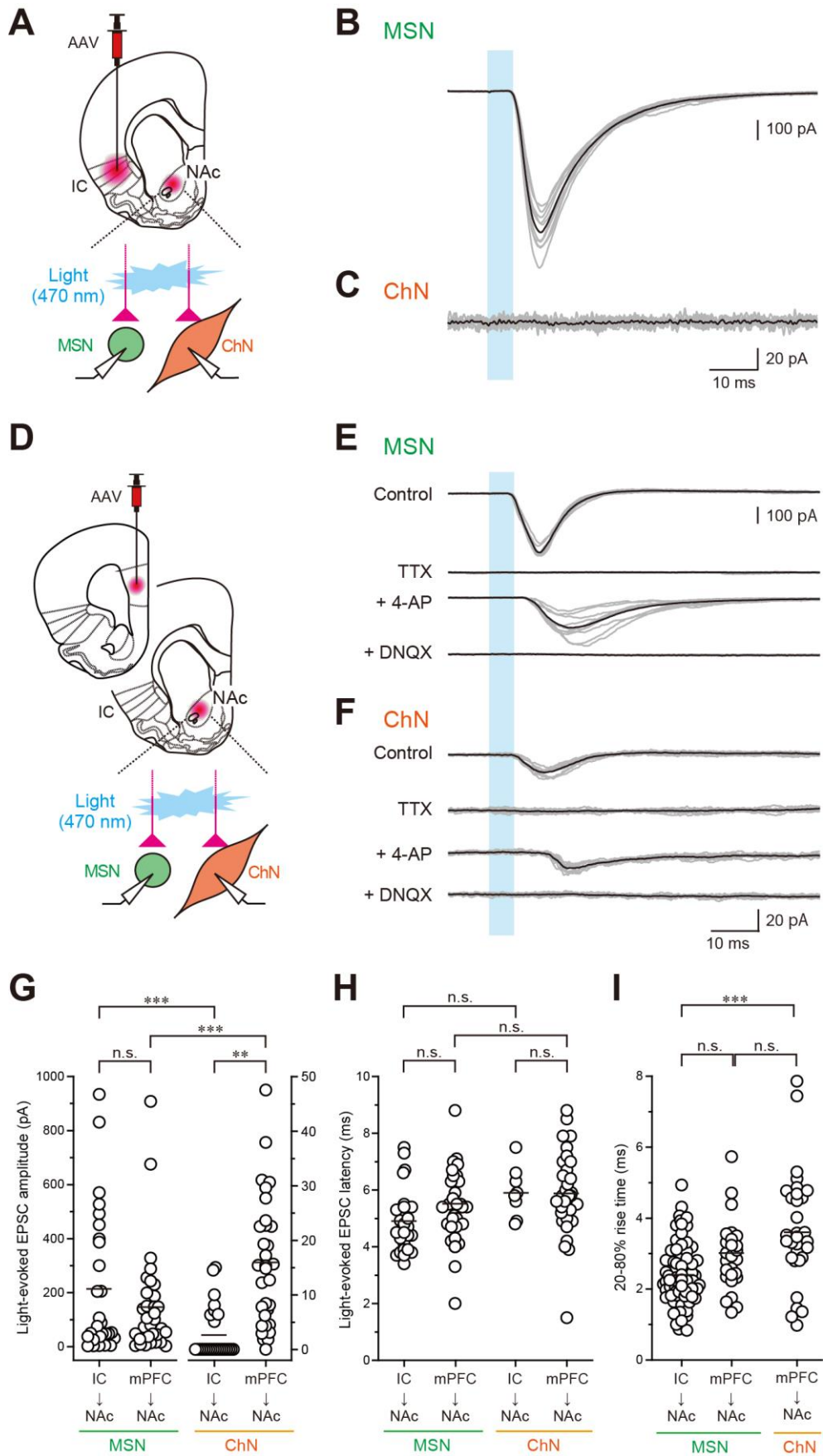


Fig. 5. EPSC profiles obtained by light stimulation of IC or mPFC axons simultaneously recorded from MSNs and ChNs. **A**, A schematic of whole-cell patch-clamp recording from an NAc MSN receiving AAV-infected IC axons. **B, C**, Paired whole-cell patch-clamp recording from an MSN (**B**) and ChN (**C**). Ten consecutive current responses (gray) are shown with their averaged traces in black. The MSNs showed light-evoked EPSCs (**B**), whereas the ChNs showed no response (**C**). **D**, A schematic of whole-cell patch-clamp recording from an NAc MSN receiving AAV-infected mPFC axons. **E, F**, Paired whole-cell patch-clamp recording from an MSN (**E**) and a ChN (**F**). Both the MSN (**E**) and ChN (**F**) showed light-evoked EPSCs. **G**, Comparison of EPSC amplitudes recorded from NAc MSNs and ChNs between the IC and mPFC. **H**, Comparison of EPSC latency values recorded from NAc MSNs and ChNs between the IC and mPFC. **I**, Comparison of EPSC rise time recorded from NAc MSNs and ChNs between the IC and mPFC. Thick horizontal bars indicate the mean. n.s., not significant, ***, $P < 0.001$, as assessed by Kruskal-Wallis ANOVA on ranks with Dunn's post hoc method (**G**) and one-way ANOVA with Tukey's post hoc test (**H** and **I**).

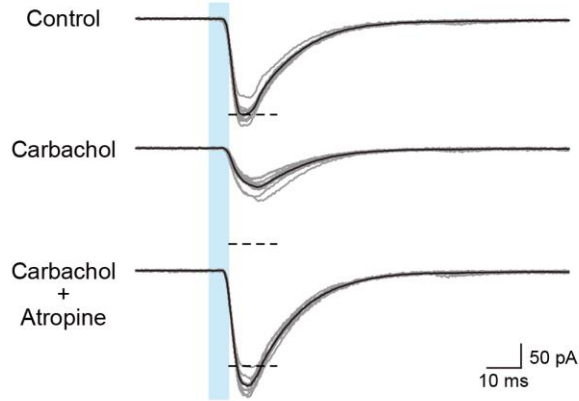
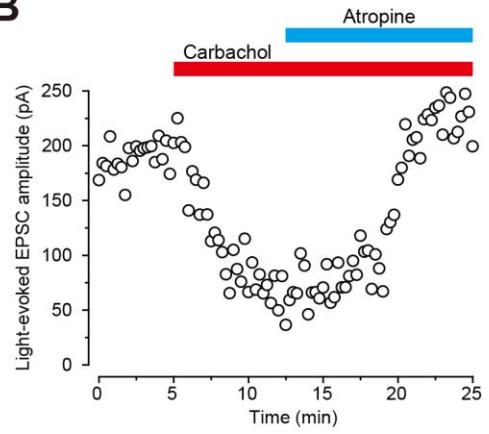
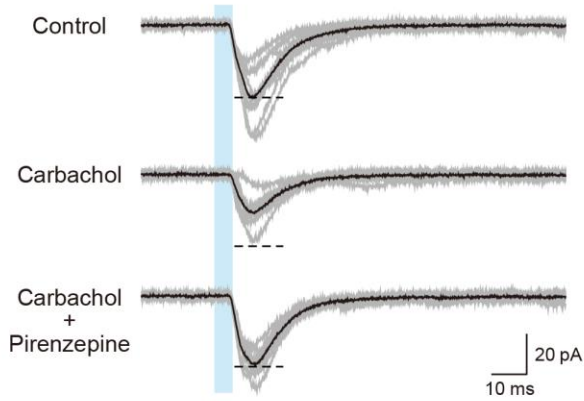
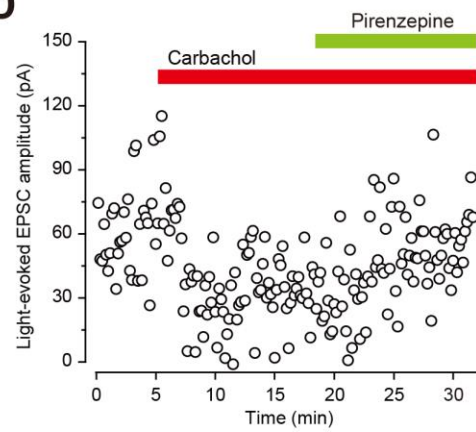
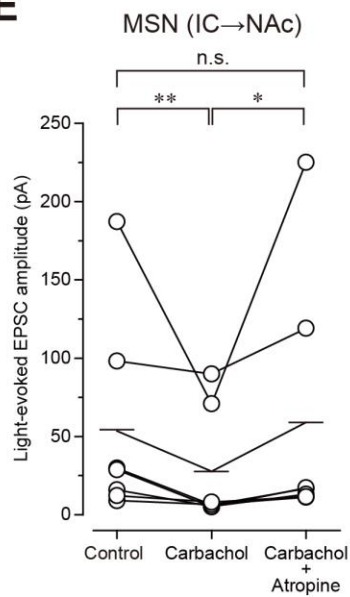
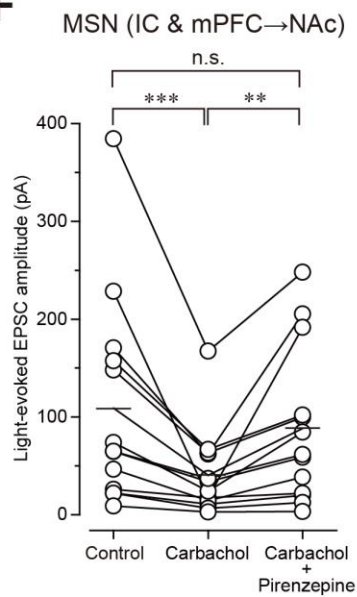
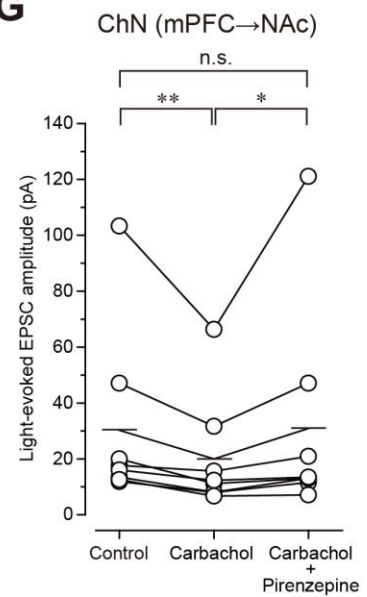
A MSN (IC→NAC)**B****C** MSN (IC→NAC)**D****E****F****G**

Fig. 6. Effects of carbachol and muscarinic antagonist on light-evoked EPSCs. **A**, A representative example of the effects of cholinergic ligands on light-evoked EPSCs in the MSN receiving AAV-infected IC axons. Carbachol (10 μ M) suppresses light-evoked EPSCs (middle), and additional application of atropine (20 μ M) rescued the suppression of EPSCs (bottom). The horizontal broken lines indicate the mean first EPSC amplitude in the control condition. **B**, The time course of the amplitude of light-evoked EPSCs before and during drug application. **C**, A representative example of the effects of cholinergic ligands on light-evoked EPSCs in the MSN receiving AAV infected IC axons. Carbachol (10 μ M) suppresses light-evoked EPSCs (middle), and additional application of pirenzepine (10 μ M) rescued the suppression of EPSCs (bottom). **D**, The time course of the amplitude of light-evoked EPSCs before and during drug application. **E**, Comparisons of the amplitude of light-evoked EPSCs in the control, during carbachol application, and during application of atropine in combination with carbachol. The results were obtained from MSNs receiving AAV-infected IC axons. **F**, Comparisons of the amplitude of light-evoked EPSCs in the control, during carbachol application, and during application of pirenzepine in combination with carbachol. The results were obtained from MSNs receiving AAV-infected IC or mPFC axons. **G**, Comparisons of the amplitudes of light-evoked EPSCs obtained from ChNs receiving AAV-infected mPFC axons. Thick horizontal bars indicate the mean. n.s., not significant, *, $P < 0.05$, **, $P < 0.01$, ***, $P < 0.001$, as assessed by Friedman's repeated measures ANOVA on ranks with Tukey's post hoc test.

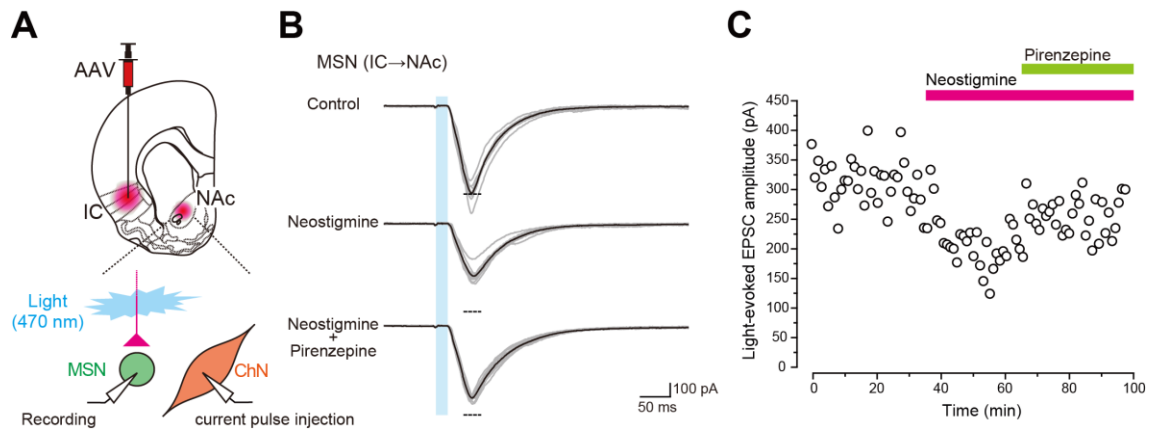


Fig. 7. Effects of neostigmine and muscarinic antagonist on light-evoked EPSCs. **A**, A schematic of whole-cell patch-clamp recording from an NAc MSN receiving AAV-infected IC axons under depolarizing current pulse injection to ChN. **B**, A representative example of the effects of cholinergic ligands on light-evoked EPSCs in the MSN receiving AAV-infected IC axons. Ten consecutive current responses (gray) with their averaged trace (black) to paired blue light stimulation (blue stripe). Neostigmine (100 μ M) suppresses light-evoked EPSCs (middle), and additional application of pirenzepine (10 μ M) rescued the suppression of EPSCs (bottom). The horizontal broken lines indicate the mean first EPSC amplitude in the control condition. **C**, The time course of the amplitude of light-evoked EPSCs before and during drug application.

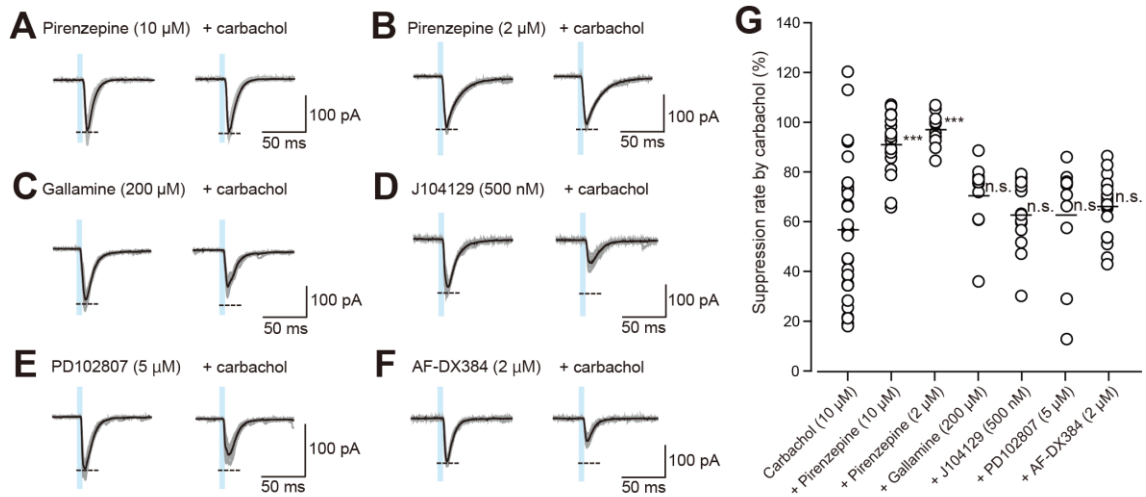


Fig. 8. Effects of $M_1/M_2/M_3/M_4$ receptor antagonists on the cholinergic suppression of light-evoked EPSCs obtained from MSNs of AAV-injected rats in the IC. **A-F**, Effects of carbachol (10 μ M) on light-evoked EPSCs under application of pirenzepine (10 μ M, **A**), pirenzepine (2 μ M, **B**), gallamine (200 μ M, **C**), J104129 (500 nM, **D**), PD102807 (5 μ M, **E**), or AF-DX384 (2 μ M, **F**). The horizontal broken lines indicate the mean EPSC amplitude under application of each antagonist. Ten consecutive current responses (gray) with their averaged trace (black) to paired blue light stimulation (blue stripe). **G**, Summary of the effects of carbachol under co-application of each antagonist. The horizontal lines indicate the mean EPSC amplitude under application of each antagonist. ***, $P < 0.001$; n.s., not significant in comparison to that in control (carbachol only) as assessed by Welch's t -test with Bonferroni correction.